Evidence of Limiting Effects of Fluctuating Potentials on V_{OC} of Cu(In, Ga)Se_2 Thin-Film Solar Cells

J.P. Teixeira,[1] P.M.P. Salomé,[2,3] B. Alves,[1] M. Edoff,[4] and J.P. Leitão[1,*]

[1] *Departamento de Física and I3N, Universidade de Aveiro, 3810-193 Aveiro, Portugal*
[2] *International Iberian Nanotechnology Laboratory, 4715-330 Braga, Portugal*
[3] *Departamento de Física, Universidade de Aveiro, 3810-193 Aveiro, Portugal*
[4] *Angström Laboratory, Solid State Electronics, Angström Solar Center, Uppsala University, Uppsala SE-751 21, Sweden*

(Received 14 December 2018; revised manuscript received 28 February 2019; published 6 May 2019)

In this paper we present a consistent theoretical approach and an extensive experimental study of Cu(In, Ga)Se_2- (CIGS-)based solar cells to investigate the influence of fluctuating potentials on the limitations of solar-cell performance. The absorptance is calculated for extensions to the Shockley-Queisser model involving the description of tail states under the Urbach-rule, optimal-fluctuation-theory, and band-gap-fluctuation models, as well as the expected values for the saturation current density, short-circuit current density, and open-circuit voltage (V_{OC}). Three CIGS-based solar cells with [Cu]/([Ga]+[In]) ratios of 0.53, 0.71, and 0.84 are grown to intentionally have sufficiently different amplitudes of fluctuating potentials. We show both theoretically and experimentally the role played by fluctuating potentials, in particular in the V_{OC} losses. We provide evidence for a higher degree of correlation of electrostatic fluctuating potentials with V_{OC} losses in comparison with band-gap fluctuations. Additionally, our results show the influence of fluctuating potentials not just at low temperature but also at room temperature.

DOI: 10.1103/PhysRevApplied.11.054013

I. INTRODUCTION

Solar cells based on a Cu(In, Ga)Se_2 (CIGS) absorber layer are the most-efficient polycrystalline solar cells, achieving a light-to-power conversion efficiency of 23.35% [1]. This remarkable electrical performance requires primarily a Cu-poor absorber composition [2–6]. The off-stoichiometry composition, in addition to the presence of four distinct atomic species in CIGS, the diffusion of atomic species (namely, Na, K, and O) from the commonly used soda-lime-glass (SLG) substrate, and the unintentional incorporation of impurities during growth, will promote local fluctuations in the composition and a large density of defects [7,8]. Any sort of perturbation of the perfect lattice will potentially contribute to the appearance of distinct energy levels in the forbidden energy band. At high densities, these defects interact with each other, resulting in a broadening of the energy levels, with possible overlap with the conduction-band and valence-band edges, forming the so-called band tails [9]. The existence of spatial fluctuations in the composition and the existence of an inhomogeneous distribution of defects (namely, charged ones) lead to band-gap (E_g) and electrostatic fluctuating potentials, respectively [10–14].

The investigation of the impact of fluctuating potentials on the performance of solar cells is presently an open issue in the scientific community [13,15–22]. Experimental studies suggest different types of fluctuations and report amplitudes of tail states [8,10,12,18,23,24]. Notwithstanding, few studies comparing the impact of different types of fluctuating potentials are available [17,19,21]. The increase of thermal generation and recombination rates due to tail states reduces the efficiency limit established in the Shockley-Queisser (SQ) model [25]. Additionally, no agreement exists concerning their influence at room temperature (RT) for CIGS-based solar cells. Several studies showed that the presence of fluctuating potentials is a factor limiting the increase of the open-circuit voltage (V_{OC}) and the solar-cell efficiency (η) [12,26]. On the other hand, for both Cu-poor $CuInSe_2$ (CIS) and Cu-poor $CuGaSe_2$, other authors claim the reduction of the amplitude of the fluctuating potentials to a few meV at RT with negligible effects on solar-cell performance [27].

In this study, we perform calculations on the influence of fluctuating potentials on the V_{OC} losses of CIGS-based solar cells according to extensions to the SQ model, and compare the predictions with experimental results. A series of three Cu-poor CIGS solar cells are grown with different Cu fraction to attain sufficiently different amplitudes of fluctuating potentials. Comparison of the theoretical

*joaquim.leitao@ua.pt

predictions with the experimental values of the V_{OC} losses provides strong support for the influence of fluctuating potentials at RT and a lower influence of band-gap fluctuating potentials on the performance of the solar cells when compared with electrostatic ones.

II. EXTENDED SQ MODELS: FLUCTUATING POTENTIALS

The SQ model establishes the upper efficiency limit of single-junction solar cells [25]. The SQ detailed balance formulation is based on the following assumptions: (a) all photons with energy $h\nu > E_g$ are absorbed, while there is no absorption of photons with energy $h\nu < E_g$; (b) each absorbed photon generates a single electron-hole pair and both charge carriers will reach their respective contacts (internal quantum efficiency of 1); (c) radiative recombination is the only loss mechanism. This model assumes a step function for the absorptance $a(h\nu)$ of the absorber layer; that is, $a(h\nu) = 1$ for $h\nu \geq E_g$ and $a(h\nu) = 0$ for $h\nu < E_g$. Under the SQ detailed balance formulation, the saturation current density (J_0^{SQ}) and the short-circuit current density (J_{SC}^{SQ}) become

$$J_0^{SQ} = q\int_0^{\infty} a(h\nu)\phi_{BB}(h\nu,T)dh\nu = q\int_{E_g}^{\infty} \phi_{BB}(h\nu,T)dh\nu, \tag{1}$$

$$J_{SC}^{SQ} = q\int_0^{\infty} a(h\nu)\phi_{Sun}(h\nu)dh\nu = q\int_{E_g}^{\infty} \phi_{Sun}(h\nu)dh\nu, \tag{2}$$

where q is the elementary charge, $\phi_{BB}(h\nu,T)$ the blackbody spectrum at the temperature (300 K) of the solar cell, and $\phi_{Sun}(h\nu)$ is the solar spectrum ($cm^{-2}\,s^{-1}\,eV^{-1}$) [28]. Then, V_{OC} may be obtained as follows:

$$V_{OC} = \frac{kT}{q}\ln\left(\frac{J_{SC}^{SQ}}{J_0^{SQ}} + 1\right), \tag{3}$$

where k is the Boltzmann constant. Because of the step function for the absorptance $a(h\nu)$, Eqs. (1) and (2) depend essentially on one input parameter related to the absorber layer (i.e., E_g), which makes this model quite simple if we think of the overall solar-cell complexity and process of operation. However, it provides a powerful starting point to address loss mechanisms other than radiative recombination [15,18,20,29–31]. On the basis of the SQ model we discuss (and compare with experimental data, see Sec. V) extensions to this model to evaluate the impact of fluctuating potentials on the solar-cell electrical parameters in the framework of each theoretical model. These extensions are also simple models that ignore other loss mechanisms existing in real devices.

It is well known that fluctuating potentials extend the density of states into the band gap, violating the SQ assumption of a step-function absorptance in which $a(h\nu) = 0$ for $h\nu < E_g$. Thus, changes in absorptance that reproduce the sub-band-gap absorption coefficient $\alpha(h\nu)$ are needed. Several theoretical approaches based on different sources of fluctuating potentials gave explicit functions for the absorption edge in the sub-band-gap region [8,12,32–34], namely: (i) the Urbach rule, (ii) optimal-fluctuation theory, and (iii) a Gaussian approach that describe the band-gap fluctuations. For the Urbach-rule model, an empirical relation is described by an exponential decay [32]:

$$\alpha(h\nu) = \alpha_0 \exp\left(\frac{h\nu - E}{E_U}\right), \tag{4}$$

where α_0 is a proportionality parameter, E is a characteristic energy parameter of the transition with a value close to the band-gap energy of the material, and E_U is an energy parameter (Urbach energy) related to the amplitude of fluctuating potentials. It is commonly assumed there are two contributions to E_U ($E_U = E_T + E_{STD}$): one arising from the thermal excitation of phonons (E_T) and another arising from static disorder (E_{STD}) [35]. In the scope of electrostatic fluctuating potentials with a spatial dimension lower than the screening length, Efros proposed [33,36] the optimal-fluctuation theory, in which the density of states exhibits a 5/4 power dependence on energy, and $\alpha(h\nu)$ is given by [12,33,36]

$$\alpha(h\nu) = \alpha_0 \exp\left[-\frac{2}{5\sqrt{\pi}}\left(\frac{E_g - h\nu}{\gamma/2}\right)^{5/4}\right], \tag{5}$$

where γ is related to the amplitude of the electrostatic fluctuating potentials. Regarding the band-gap fluctuations, a model [8,12] assumes a Gaussian distribution of local band gaps (E_g^{loc}) around a mean value, E_g^{mean}, with a standard deviation σ, and gives

$$\alpha(h\nu) = \alpha_0 \int_0^{\infty} \frac{1}{\sigma\sqrt{2\pi}}\exp\left[-\frac{1}{2}\left(\frac{E_g^{loc} - E_g^{mean}}{\sigma}\right)^2\right] \times \left(\frac{\sqrt{h\nu - E_g^{loc}}}{h\nu}\right) dE_g^{loc}. \tag{6}$$

The existence of explicit functions for the absorption coefficient that deal with a particular type of fluctuating potentials [Eqs. (5) and (6)] allows the investigation of separate contributions to solar-cell electrical parameters. In the following, we start by addressing different approaches to obtain $a(h\nu)$.

For the Urbach-rule model, we adapt the approach of Jean *et al.* [18] to a planar solar cell and assume zero front reflectance and total reflection on the rear side. Thus, the absorptance follows the Lambert-Beer law [20,37–39]:

$$a(h\nu) = 1 - \exp[-2\alpha(h\nu)W], \tag{7}$$

where $\alpha(h\nu)$ is given by Eq. (4) and W is the thickness of the absorber layer. In the case of electrostatic fluctuating potentials, we again adapt the approach of Jean *et al.* [18]. For $h\nu < E_g$, $a(h\nu)$ is modeled for a planar solar cell, and the total $a(h\nu)$ is given by

$$a(h\nu) = \begin{cases} 1 - \exp[-2\alpha(h\nu)W], & h\nu < E_g, \\ 1, & h\nu \geq E_g, \end{cases} \tag{8}$$

where $\alpha(h\nu)$ is given by Eq. (5).

Finally, in comparison with the electrostatic fluctuating potentials, for the band-gap ones, $a(h\nu)$ must take into account that spatial fluctuations in the composition will cause local changes in the band gap, which should be reflected in the modulation of $a(h\nu)$ below and above the band-gap energy. Rau and Werner [29] represented the absorptance dependence on σ as follows:

$$a(h\nu) = \frac{1}{2}\,\mathrm{erfc}\left(\frac{E_g^{\mathrm{mean}} - h\nu}{\sigma\sqrt{2}}\right). \tag{9}$$

There is an important difference between the previous three theoretical models. Whereas, optimal-fluctuation theory and the Gaussian models focus on particular types of fluctuating potentials, the Urbach rule reflects the influence of shallow tail states, but it is not clear if this model is able to distinguish the different types of fluctuating potentials, since it is an empirical model. The impact of fluctuating potentials described by the Urbach-rule model on the performance of the solar cell may be discussed by replacing the step function $a(h\nu)$, proposed by Shockley and Queisser, by Eq. (7) in Eqs. (1) and (2), to obtain J_0^{Urbach} and $J_{\mathrm{SC}}^{\mathrm{Urbach}}$, respectively. The remaining solar-cell electrical parameters are obtained following the usual procedure. Furthermore, to study the balance of the influence of electrostatic fluctuating potentials and band-gap ones, $a(h\nu)$ is given by Eqs. (8) and (9), respectively. Comparison of the SQ electrical parameters, which set the upper limit, with the electrical parameters obtained by the SQ extensions allows us to discuss the losses induced by fluctuating potentials and, more importantly, to discuss the contribution given by electrostatic and band-gap fluctuating potentials.

III. EXPERIMENTAL METHODS

A set of three Cu-poor CIGS solar cells are fabricated following a modified version of the Ångstrom solar cell baseline [40]. Flat evaporation rates are used to achieve Cu-poor samples with [Cu]/([Ga]+[In]) ratios of 0.53, 0.71, and 0.84 (from now on denoted by Cu53, Cu71, and Cu84, respectively). The [Ga]/([Ga]+[In]) ratio was fixed at 0.3, without any Ga profile in depth. Both composition rates are in accordance with the nominal composition. Following the literature [3], the composition of the CIGS films is determined by x-ray fluorescence and is performed with a PANalytical Epsilon 5 spectrometer. Structural analysis by x-ray diffraction (XRD) is performed with a PANalytical X'Pert PRO MRD diffractometer equipped with a Cu Kα source ($\lambda = 1.54060$ Å) in the Bragg-Brentano configuration. The diffractograms obtained (see Supplemental Material [41] and Ref. [42]) show that the absorber layers in all three samples are clearly dominated by the CIGS phase (α phase). In the case of the Cu53 sample, a trace of the $CuIn_3Se_5$ phase (β phase) is detected. The thicknesses (W) of the CIGS layers are obtained by stylus profilometry, and are 1.82, 1.88, and 2.07 μm for the Cu53, Cu71, and Cu84 samples, respectively. After deposition of the buffer layer, each sample is split into two adjacent pieces. One of them, with the structure SLG/Mo/CIGS/CdS, is used for photoluminescence (PL) measurements, whereas in the other the solar-cell structure (SLG/Mo/CIGS/CdS/i-ZnO/ZnO:Al/Al grid) is completed. The morphology of the complete solar cells is investigated by scanning electron microscopy, with a FEI Quanta 650 FEG instrument. Cross-section images (see Supplemental Material [41]) show similar grain sizes for the Cu53 and Cu71 samples, whereas a great increase is observed for the Cu84 sample.

The optical characterization is performed through PL and external quantum efficiency (EQE). The PL measurements are performed with a Bruker IFS 66v Fourier-transform infrared spectrometer equipped with a Ge-diode detector. The excitation wavelength is the 514.5-nm line of an Ar^+-ion laser (spot diameter of approximately 1 mm). The laser power is measured at the front of the cryostat window. The excitation power ranges from 0.09 mW (3.0×10^{16} photons s^{-1} cm^{-2}) to 30 mW (9.9×10^{18} photons s^{-1} cm^{-2}). The correction of the detectivity of the Ge detector is performed for all spectra. No influence of an interference effect is observed in the PL spectra [43]. We measure EQE with a homebuilt system with a xenon lamp using chopped monochromatic light in the wavelength range from 360 to 1200 nm in 2-nm steps.

Complete solar cells are characterized by measurements of current density versus voltage (J-V) with illumination by an ELH lamp calibrated to AM1.5g conditions with use of an in-house system. The electrical parameters presented are the average across ten solar cells for each sample.

IV. EXPERIMENTAL RESULTS

Figure 1(a) shows the PL spectra of the three samples measured at 7 K with an excitation power of 10 mW

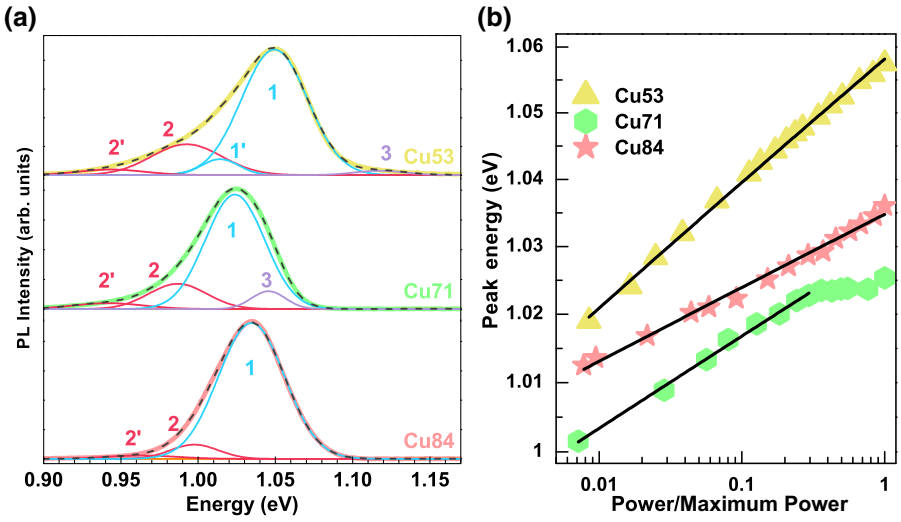

FIG. 1. (a) PL spectra of the Cu53, Cu71, and Cu84 samples measured at 7 K with an excitation power of 10 mW (3.3×10^{18} photons s^{-1} cm^{-2}). The fitting models with Gaussian components are shown for each sample. Gaussian components 1 and 1′ are ascribed to the main transition, whereas Gaussian components 2 and 3 are ascribed to the lower- and higher-energy transitions, respectively. (b) Dependence of peak energy of transition 1 on the normalized excitation power for the three samples. The solid lines represents the fit of Eq. (10) to the experimental data.

(3.3×10^{18} photons s^{-1} cm^{-2}). For all Cu fractions the luminescence is broad and asymmetric. From the overall behavior of the luminescence as a function of the excitation power (discussed below), clear evidence for more than one radiative transition is obtained for each sample. The deconvolution of the PL spectra was done by assuming Gaussian components. The fitting model for each sample comprises the lowest number of components required to describe the luminescence in the whole PL spectra. More details are given in Supplemental Material [41] and Refs. [9,13,44,45]. Two transitions are identified for the Cu84 sample (transitions 1 and 2), while for the Cu71 and Cu53 samples a third transition (transition 3) is observed at higher energies. Transitions 2 and 3 are described by two Gaussian components [denoted by 2 and 2′ in Fig. 1(a)] and one Gaussian component, respectively. Transition 1 is well described by just one Gaussian component in the Cu73 and Cu84 samples. However, to use the same fitting model throughout the dependence of the luminescence on excitation power (P) of the Cu53 sample, a second Gaussian component [denoted by 1′ in Fig. 1(a)] is needed. From now on, we focus on the main radiative transition (transition 1) as its peak energy (E_p) is representative of the experimental behavior of the whole luminescence.

The E_p values of transition 1 for each sample obtained for the aforementioned measurement conditions are shown in Table I. No straightforward dependence on the Cu fraction is observed. Two factors can be responsible for a shift in the energy of the luminescence between samples: a change of the band-gap energy and/or a change in the influence of fluctuating potentials, as a consequence of different densities of charged defects, and structural inhomogeneities [8,13,46]. However, neither of them alone can explain the experimental trend as shown in the following. To address the first issue, EQE measurements are performed. The linear fit to the data in the plot of EQE^2 versus $h\nu$ for a range of approximately 0.2–0.39, shown in Fig. 2(a), provides band-gap energies of 1.20 ± 0.10 eV, 1.14 ± 0.05 eV, and 1.10 ± 0.02 eV for the Cu53, Cu71, and Cu84 samples, respectively. In the case of the Cu53 sample, the high error can be compatible with the presence of a trace of the $CuIn_3Se_5$ phase observed in the XRD measurements. Despite not being absolute values of the band-gap energy, they enable comparison between samples. For that reason, those values are assumed to be the effective band gaps of the samples and used in all the following calculations. As expected, the band-gap energy decreases with the increase of the Cu fraction due to the increase in the repulsive interaction between Cu $3d$ and Se $4p$ states, which defines primarily the maximum of the valence band in CIGS [46–48]. However, the dependence of the band gap on the Cu fraction obtained does not

TABLE I. Composition and optical and electrical parameters obtained for the three samples. [Cu]/([Ga]+[In]) (CGI) and [Ga]/([Ga]+[In]) ratios estimated from x-ray-fluorescence measurements, peak energy for transition 1 ($E_{p,1}$) and β estimated from PL spectra, band-gap energy (E_g) obtained from plots of EQE^2 versus $h\nu$, and J_{SC}, V_{OC}, fill factor (FF), and η estimated from the J-V curves. The calculated V_{OC} losses (E_g/q-V_{OC}) are shown. The $E_{p,1}$ values are estimated from PL spectra measured at 7 K with an excitation power of 10 mW (3.3×10^{18} photons s^{-1} cm^{-2}).

Sample	CGI ratio	GGI ratio	$E_{p,1}$ (eV)	E_g (eV)	β (meV)	J_{SC} (mA cm^{-2})	V_{OC} (mV)	FF (%)	η (%)	$E_g/q - V_{OC}$ (mV)
Cu53	0.53	0.31	1.049 ± 0.001	1.20 ± 0.10	8.1 ± 0.1	30.04 ± 0.24	502 ± 12	70.4 ± 0.6	10.5 ± 0.3	698
Cu71	0.71	0.30	1.024 ± 0.001	1.14 ± 0.05	5.8 ± 0.1	31.82 ± 0.49	570 ± 10	76.3 ± 3.9	13.8 ± 0.9	570
Cu84	0.84	0.30	1.035 ± 0.001	1.10 ± 0.02	4.7 ± 0.1	32.30 ± 0.26	600 ± 5	77.4 ± 0.9	15.1 ± 0.3	500

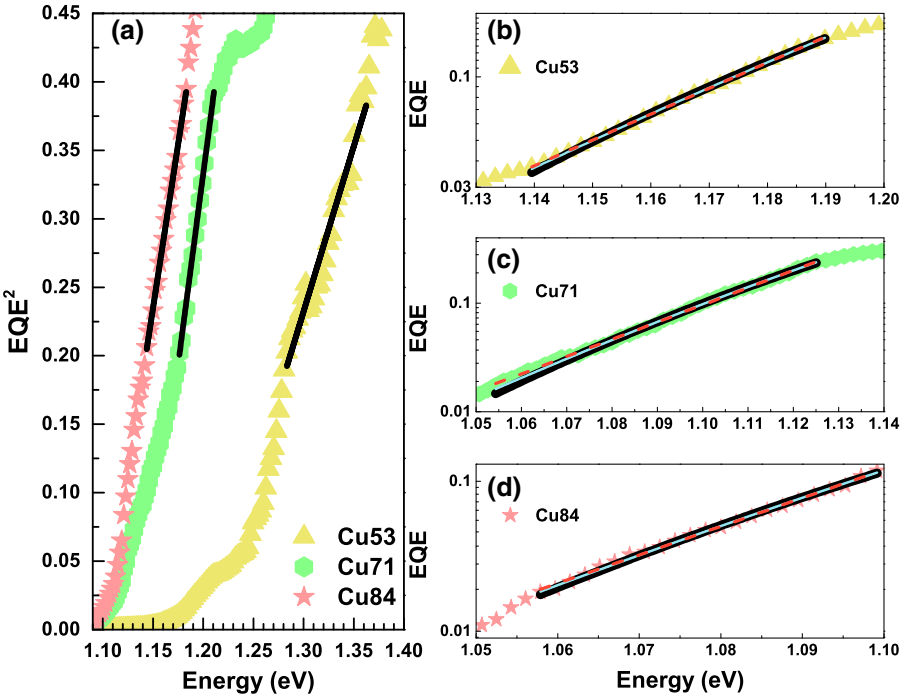

FIG. 2. (a) Plots of EQE^2 versus $h\nu$ for the three samples depicting a linear fit for the estimation of the band-gap energies. (b)–(d) Sub-band-gap energy range of the EQE plot for the Cu53, Cu71, and Cu84 samples. The solid black, solid cyan, and dashed orange lines represent the fit of Eqs. (6), (4), and (5), respectively, to the experimental data.

follow the dependence observed for the shift of the peak energy (see Table I). We now focus on the possible influence of fluctuating potentials on the energy shift of the luminescence, starting by studying the dependence of the luminescence on P. As P increases, a blueshift of the emission is observed for all samples, as shown in Fig. 1(b) (see also Supplemental Material [41]). In the literature, the dependence on P of E_p is often described by the following relation [49–52]:

$$E_p = \beta \ln\left(\frac{P}{P_0}\right), \tag{10}$$

where β characterizes the energy shift and P_0 is a fitting parameter. To a great extent, β reflects the amplitude of the overall fluctuating potentials, as discussed by Yu and Park [49]. Estimated β values of 8.1 ± 0.1 meV, 5.8 ± 0.1 meV, and 4.7 ± 0.1 meV for the Cu53, Cu71, and Cu84 samples, respectively, are obtained. Such high β values are compatible with the existence of fluctuating potentials [13,49–51,51,52]. The decrease of β with the increase of the Cu fraction is in accordance with the proposed aim to grow a set of CIGS solar cells with sufficiently different amplitudes of fluctuating potentials. Nevertheless, the monotonous trend of estimated β values does not follow the experimental E_p behavior. Thus, the energy shift of the luminescence should reflect both of the previous factors.

The temperature range in the PL study is far from the operation temperatures of the solar cells. Thus, it is important to correlate the existence of fluctuating potentials at low temperature with their possible existence at RT. In this way, we study the sub-band-gap energy range of the EQE plot (measured at RT). For that energy range, EQE is proportional to the absorption coefficient and follows the density of states of fluctuating potentials. Following the above discussion of the SQ extensions (Sec. II), the sub-band-gap energy range of the EQE plot for the Cu53, Cu71, and Cu84 samples is tentatively fitted with Eqs. (4)–(6). In the case of the Cu84 sample, the fits are performed until the band gap, whereas for the other two samples none of the theoretical models is able to fit the whole sub-band-gap range. For the Cu53 and Cu71 samples, two energy regions may be identified: a narrow one close to the band gap (corresponding to a few experimental points), which reflects shallow tails, and another one, involving deeper tails. The latter type of tails is the one that has a stronger impact on the performance of the device and thus the one that is more relevant for our study. The resulting fits are shown in Figs. 2(b)–2(d) and the parameters obtained that describe the amplitude of fluctuating potentials are presented in Table II (for additional details, see Supplemental Material [41]). The fits show that the three different equations fit the same EQE region for each sample fairly well. This result is a consequence of the presence in the sub-band-gap region of tails with

TABLE II. Values of E_U, γ, and σ obtained from the fits of Eqs. (4), (5), and (6), respectively, to the sub-band-gap energy range of the EQE plot.

Sample	E_U (meV)	γ (meV)	σ (meV)
Cu53	35.5 ± 0.2	32.2 ± 0.2	68 ± 7
Cu71	27.4 ± 0.2	24.3 ± 0.2	65 ± 5
Cu84	22.9 ± 0.2	21.4 ± 0.3	54 ± 10

different amplitudes. Thus, the dependence on energy of the total density-of-states function is not purely exponential, Gaussian, etc. [53]. The E_U values obtained are in agreement with the values previously reported for CIGS [54–58]. Also, the observed decrease of the estimated E_U values with the increase of the Cu fraction is in accordance with the findings of the work of Sioda *et al.* [54], in which a series of CIS samples were evaluated. However, in that work, the Cu-fraction range studied for Cu-poor samples was smaller than in our case and closer to the stoichiometry. The values of γ (electrostatic fluctuating potentials) obtained decrease with the increase of the Cu fraction, and are also in agreement with the values reported by other authors [10,12]. Dirnstorfer *et al.* [10] showed a similar behavior for γ for a different Cu-fraction range. Lastly, our estimated σ values (band-gap fluctuating potentials) also decrease with the increase of the Cu fraction, and are higher than previously reported values [12].

The theoretical models presented do not provide absolute values for the amplitude of fluctuating potentials. Indeed, in Table II, the E_U values are higher than the values obtained for γ, which reflects the qualitative nature of these parameters, since the exponential function that describes the Urbach-rule model should deal with shallower tail states than the ones described by the power 5/4 function in the scope of the optimal-fluctuation theory. Thus, E_U, γ, and σ values should not be directly ascribed to the effective amplitude of tail states, it being possible to compare their values only within each particular model. Moreover, the values obtained from different experimental techniques, even being equivalent, should not be compared straightforwardly, as shown by Malerba *et al.* [59]: for Cu_2ZnSnS_4, they obtained significantly different values for E_U from the absorption spectrum and the EQE plot.

The dependence on the Cu fraction of E_U, γ, and σ (estimated at RT) follows the same dependence of β (estimated at low temperature). This is an important result due to the differences in physical and mathematical approaches used in the theoretical models, and also because of the different temperatures at which the measurements were taken. Thus, our results strongly suggest that temperature is not a limiting factor for the discussion of the influence of fluctuating potentials, which follows previous results presented by Shioda *et al.* [54] and Wasim *et al.* [60] for CIS and by Troviano and Taretto [57] for Cu-poor CIGS, for which the dependence of E_U on the temperature in the ranges 90–300 K and 150–300 K, respectively, was studied. Whereas for CIS a weak increase of E_U was obtained with the increase of temperature (Cu-poor CIS, $\Delta E_U \sim 3$ meV; Cu-rich CIS, $\Delta E_U \sim 4$ meV [54]), for CIGS, E_U remained almost constant in the whole temperature range investigated. Finally, our results also suggest a decrease in the density of charged defects as the Cu fraction increases. However, a relation with the net doping is difficult to establish, due to the different degrees of compensation of the three samples.

The electrical characterization of the solar cells is summarized in Table I. The increase of the Cu fraction leads to an increase of 2.26 mA cm^{-2} in J_{SC}, 98 mV in V_{OC}, and 7% in the fill factor (FF), resulting in a 4.6% higher light-to-power conversion efficiency for the Cu84 sample in comparison with the Cu53 sample. Thus, all electrical parameters, as well as the performance of the solar cells, improve with the increase of the Cu fraction. This behavior is in accordance with the [Cu]/([Ga]+[In]) ratios (0.88–0.92) reported in the literature for the best solar cells [61].

In Fig. 3(a), both the experimental (J_{SC}^{exp}) and the upper theoretical (J_{SC}^{SQ}) J_{SC} values are plotted as a function of

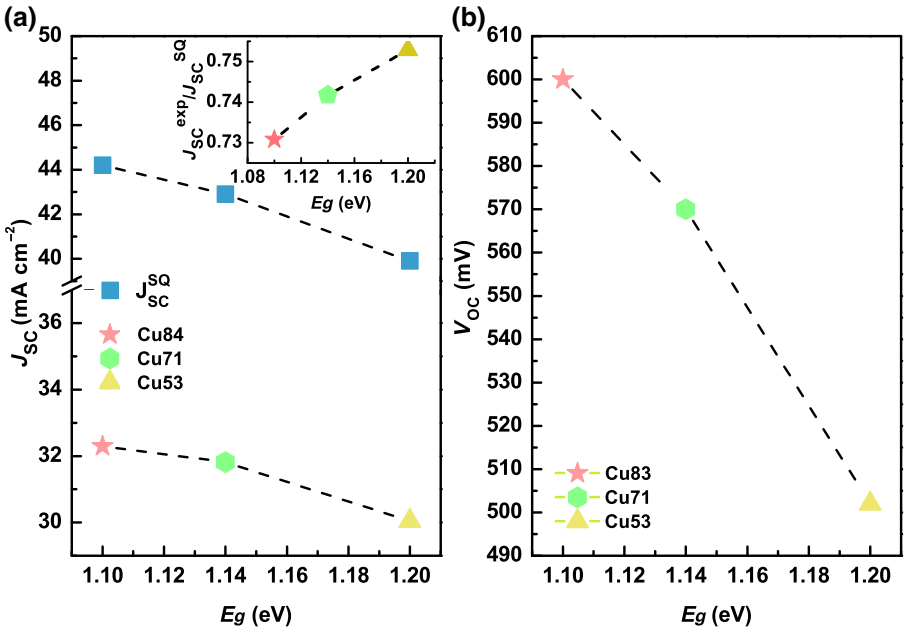

FIG. 3. Dependence of (a) J_{SC}^{exp} and J_{SC}^{SQ} and (b) V_{OC} on the band-gap energy. The inset in (a) shows the dependence of the J_{SC}^{exp}/J_{SC}^{SQ} ratio on the band-gap energy.

the estimated band-gap energies. As expected, J_{SC}^{exp} for the three samples is lower than the maximum theoretical value, and follows the theoretical trend. The inset in Fig. 3(a) shows the dependence of the J_{SC}^{exp}/J_{SC}^{SQ} ratio on the band-gap energy. Despite the increase of 2.26 mA cm^{-2} in J_{SC}^{exp} with the increase of the Cu fraction, the J_{SC} loss in comparison with J_{SC}^{SQ} is lower for the Cu53 sample and increases with the increase of the Cu fraction. This result suggests that the improvement in the performance of the solar cells with the increase of the Cu fraction is not related to an effective increase in J_{SC}. At this point, we note that the correlation of J_{SC}^{exp} with the impact of fluctuating potentials is not straightforward. A decrease in the density of defects will potentially increase the diffusion length and the space-charge region, which contributes to an increase of the collection function. Nevertheless, such a decrease of the density of defects will create smaller fluctuating potentials that contribute to less absorption below the band-gap energy. Thus, any correlation must be only qualitative.

Figure 3(b) shows the dependence of V_{OC} on the band-gap energy. Theoretically, it is expected that V_{OC} follows the band gap. However, this is not the case for our samples. Among other reasons, different factors contribute to the V_{OC} losses (E_g/q-V_{OC}): (i) the presence of fluctuating potentials; (ii) native point defects inside the band gap; (iii) the presence of secondary phases with a band-gap energy lower than that of CIGS; (iv) the polycrystalline character of the absorber layer, which will favor the diminishing of the lifetime of photogenerated carriers and, consequently, of their collection; (v) interface recombination; and (vi) misalignments of energy bands at interfaces between the different solar-cell layers. Indeed, most of these limiting factors are related to the presence of defects, and their influence on the V_{OC} losses is twofold. They contribute to a reduction of the band-gap energy in comparison with the nondoped semiconductor due to a renormalization effect [62–64]. The occurrence of tails in the conduction and valence bands is reflected in a non-step-like absorptance. Consequently, absorption below the band gap occurs, and is described by the radiative losses in V_{OC}. Additionally, the existence of a large density of defects, with relevance for the charged defects, creates nonradiative recombination channels that contribute to nonradiative losses in V_{OC} [65].

As discussed above, a high density of defects can strongly reduce V_{OC}, while J_{SC} can be less affected [66]. We find a decrease in the density of defects as the Cu fraction increases, which is compatible with a lower influence of fluctuating potentials in the Cu84 sample. Thus, to evaluate the importance of fluctuating potentials in the V_{OC} losses, these losses are plotted in Fig. 4. Additionally, similar plots of the estimated β, γ, E_U, and σ values are included. As noted previously, the absolute values of these parameters cannot be compared between each other, and only values of a particular parameter (for a particular model) can be compared between samples in the same

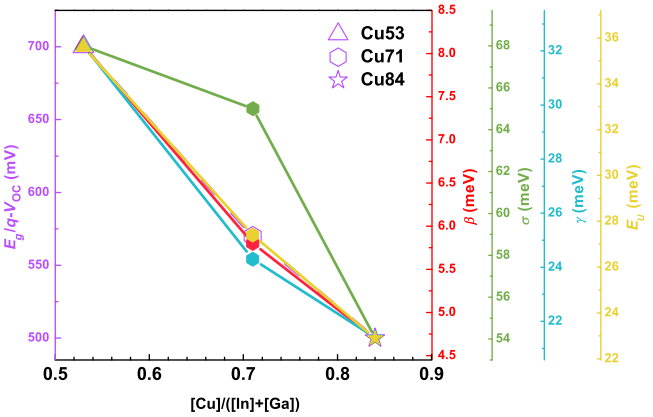

FIG. 4. V_{OC} losses and parameters (β, σ, γ, and E_U) proportional to fluctuating potentials for each sample.

experiment. To allow such a comparison, in Fig. 4 we do match the experimental values estimated for the different models used for the samples with the extreme Cu fractions. It is expected that β and E_U reflect the amplitude of fluctuating potentials of different origins (electrostatic, band gap, thermal vibration, etc.) in the sample. As shown in Fig. 4, the V_{OC} losses correlates with the band tails caused by potential fluctuations, which is compatible with reports for different materials [67]. Our results show that β and E_U are the parameters that best describe experimental V_{OC} losses. Moreover, the γ values obtained also follow quite well the experimental V_{OC} losses, even though they characterize only the amplitude of electrostatic fluctuating potentials. Finally, for values of σ, which reflects only the band-gap fluctuations, the behavior is significantly different. Thus, our results show unequivocally that (i) fluctuating potentials are a deciding factor for the V_{OC} losses and (ii) the electrostatic fluctuating potentials are in a higher degree of correlation with experimental data than the band-gap fluctuations.

V. COMPARISON WITH THE SQ MODEL AND SQ EXTENSIONS

The basic principles of operation of solar cells may be summarized as a three-step process: (i) absorption of light and generation of an electron-hole pair; (ii) separation of the electron-hole pair; and (iii) collection of the electron and hole in the opposite contacts. Fluctuating potentials should have an impact on all three processes. However, with the SQ extensions discussed in Sec. II, we focus only on the first of the three processes. We calculate the electrical parameters given by the SQ model as well as its extensions. As a first step, the absorptance must be evaluated for all models according to Eqs. (7)–(9), the relevant parameters being presented in Table II (for α_0, see Supplemental Material [41]). In Fig. 5, we illustrate for the Cu84 sample the energy dependence of the absorptance for all theoretical models, assuming $E_g = 1.10$ eV. For

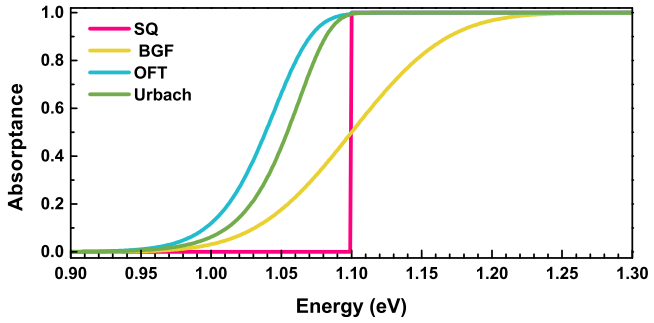

FIG. 5. Absorptance spectra for the Cu84 sample calculated with the SQ, band-gap-fluctuation (BGF), optimal-fluctuation-theory (OFT), and Urbach-rule models. A value of $\alpha_0 = 1.24 \times 10^4$ cm^{-1} is estimated with use of the data of Paulson *et al.* [68] (for more details, see Supplemental Material [41]).

the optimal-fluctuation-theory and Urbach-rule models, the correction to the SQ absorptance occurs only in the sub-band-gap energy range, whereas for the band-gap-fluctuation model, the correction is centered at the band-gap energy. Thus, from the energy dependence of the absorptance obtained, we may state that the Urbach-rule model should follow to a great extent the influence of the electrostatic fluctuating potentials.

The resulting electrical parameters are calculated with the theoretical models and are presented in Table III. A few trends can be identified. On average, for all samples, the J_{SC}^{SQ} and J_0^{SQ} values are lower than the values estimated by the SQ extensions. This observation may be understood by combining the absorption of photons below the band-gap energy with the shape of the solar spectrum, which can result in more photons being collected and thus contributing to the photocurrent. However, this result is compatible with the impact of the fluctuating potentials in J_{SC}, as discussed above. Indeed, the optimal-fluctuation-theory model, is the one for which the absorptance extends more to lower energy values (see Fig. 5), resulting in more total absorption of photons and providing the highest J_{SC} values of all. For the V_{OC} values, for the SQ extensions, a significant and expected reduction is observed when fluctuating potentials are taken into account. The V_{OC} losses are greater for the Cu53 sample and decrease with increase of the Cu fraction.

In Fig. 6 we compare the calculated V_{OC} losses with the experimental values, following the same approach used to build Fig. 4. We observe that the V_{OC} losses calculated by the SQ model follow quite well the experimental ones, the V_{OC} losses calculated by the Urbach-rule and optimal-fluctuation-theory models follow reasonably well the experimental values, and the V_{OC} losses calculated by the band-gap-fluctuation model reveal a disagreement. These observations are highly compatible with the experimental results (see Fig. 4). At this stage, we stress that the main differences between the three samples are the band-gap energies and the influence of fluctuating potentials in each one. In the SQ model, only the first issue is addressed, whereas both issues are included in the Urbach-rule and optimal-fluctuation-theory models. That the SQ model closely follows the experimental values in Fig. 6 is expected because it is well known that this model describes quite well the basic principles of operation of a solar cell. In addition, this agreement validates the approach to use the SQ model as a starting point for the study of other loss mechanisms rather than just the radiative ones as proposed in the SQ model. Nevertheless, the V_{OC} losses calculated with the SQ model (Table III) are the losses that deviate most from the experimental losses. Regarding the extensions to the SQ model, the inclusion of fluctuating potentials reveals that as for the case of the Urbach rule and optimal-fluctuation theory, the experimental trend can be described. For the band-gap-fluctuation model, the disagreement is quite evident and unexpected. Different factors may be contributing to this behavior: (i) negligible influence of the band-gap fluctuations in comparison

TABLE III. J_{SC}, J_0, V_{OC}, and E_g/q-V_{OC} values calculated with the SQ, optimal-fluctuation-theory (OFT), band-gap-fluctuation (BGF), and Urbach-rule models. The values of E_g (see Table I) are also shown for each sample. α_0 was estimated by fitting Eq. (S1) to the absorption-coefficient data of Paulson *et al.* [68] (see Supplemental Material [41]).

Sample	E_g	Model	J_{SC} (mA cm^{-2})	J_0 (mA cm^{-2})	V_{OC} (mV)	E_g/q-V_{OC} (mV)
Cu53	1.20 ± 0.10	SQ	39.97	4.23×10^{-15}	951	249
		BGF	40.02	9.94×10^{-14}	869	331
		OFT	43.92	2.86×10^{-12}	785	415
		Urbach rule	43.24	9.41×10^{-11}	694	506
Cu71	1.14 ± 0.05	SQ	42.89	3.84×10^{-14}	896	244
		BGF	42.53	6.88×10^{-13}	821	319
		OFT	45.17	1.98×10^{-12}	795	345
		Urbach rule	44.79	4.87×10^{-12}	772	368
Cu84	1.10 ± 0.02	SQ	44.23	1.71×10^{-13}	858	242
		BGF	44.12	1.24×10^{-12}	807	293
		OFT	46.45	4.68×10^{-12}	774	326
		Urbach rule	45.81	3.88×10^{-12}	778	322

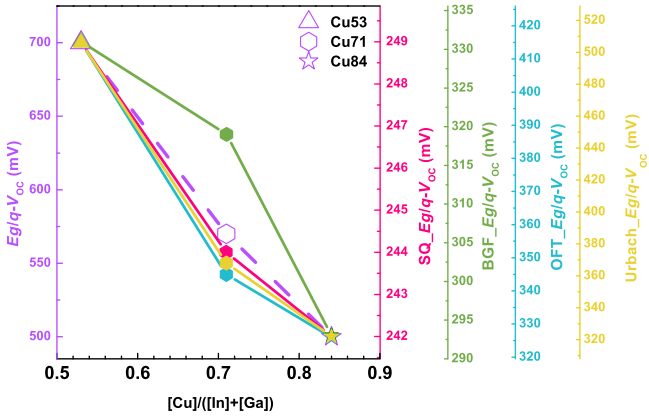

FIG. 6. V_{OC} losses obtained experimentally and calculated with the SQ, band-gap-fluctuation, optimal-fluctuation-theory, and Urbach-rule models for each sample.

with the electrostatic one; (ii) EQE and PL measurements are not sensitive enough to the band-gap fluctuating potentials, which is questionable because the two experimental techniques have different physical principles; and (iii) the theoretical model need to be improved to better describe fluctuations of this type.

The fact that the V_{OC} losses calculated by the optimal-fluctuating-theory and Urbach-rule models follows the experimental values for γ and E_U shows that the approximation to a planar solar cell and the proposed $a(h\nu)$ are good approximations to evaluate the impact of the fluctuating potentials on solar cells. As discussed above, many factors may and likely do contribute to the V_{OC} losses. Even though we cannot fully account for the experimental V_{OC} losses, our results support the experimental correlation between them and the presence of fluctuating potentials.

The experimental results and theoretical approaches presented show a clear correlation between electrostatic fluctuating potentials and V_{OC} losses on the devices studied. To obtain CIGS-based devices with a significantly different influence of fluctuating potentials, we vary the Cu fraction. Thus, for our set of samples, the origin of the charged defects that greatly contribute to electrostatic fluctuating potentials will certainly have an influence on several factors, including intrinsic defects, deviation from stoichiometry, incorporation of impurities, grain boundaries, and interface defects. It is well known that the Cu fraction has a major influence on the density of defects as well as on the grain size in CIGS. Nevertheless, the Cu53 and Cu71 samples have similar grains sizes (see Supplemental Material [41]), whereas in the case of the Cu84 sample, a great increase in the size is observed. Thus, for this particular sample, we expect a lower contribution of grain boundaries for the electrostatic fluctuating potentials. However, we believe that the dependence of the defect formation energy on the composition is the major factor that contributes to the electrostatic fluctuating potentials in the series of samples studied [46].

VI. CONCLUSIONS

In this work, we provide strong evidence based on a theoretical approach and experimental results that the V_{OC} losses of CIGS solar cells are correlated with the amount of fluctuating potentials in the absorber layer. Evidence for a lower influence of band-gap fluctuating potentials, in comparison with electrostatic ones, was found. Furthermore, the fluctuations estimated from low-temperature PL measurements, which are very sensitive to the general influence of defects in semiconductors, are in accordance with standard EQE measurements at RT. Having established that correlation and a way to measure it, the next steps are to quantify, identify, and analyze state-of-the-art CIGS devices to evaluate losses.

ACKNOWLEDGMENTS

The authors thank José M. Castanheira for useful discussions. This research was funded by FEDER funds through the COMPETE 2020 program and National Funds through Fundação para a Ciência e a Tecnologia (FCT) under Projects No. UID/CTM/50025/2013 and No. POCI-01-0145-FEDER-007688, by the Development of Novel Ultrathin Solar-Cell Architectures for Low-Light, Low-Cost and Flexible Optoelectronic Devices project (Project No. 028075) cofunded by FCT and the ERDF through the COMPETE 2020 program, and by Project No. CENTRO-01-0145-FEDER-000005 (SusPhotoSolutions—Soluções Fotovoltaicas Sustentáveis). P.M.P.S. acknowledges the funding by FCT through Project No. IF/00133/2015.

[1] Solar Frontier, Press Release, Japan, January 17, 2019.
[2] R. Noufi, R. Axton, C. Herrington, and S. K. Deb, Electronic properties versus composition of thin films of $CuInSe_2$, Appl. Phys. Lett. **45**, 668 (1984).
[3] S. Niki, M. Contreras, I. Repins, M. Powalla, K. Kushiya, S. Ishizuka, and K. Matsubara, CIGS absorbers and processes, Prog. Photovoltaics Res. Appl. **18**, 453 (2010).
[4] P. M. P. Salomé, V. Fjällström, P. Szaniawski, J. P. Leitão, A. Hultqvist, P. A. Fernandes, J. P. Teixeira, B. P. Falcão, U. Zimmermann, A. F. da Cunha, and M. Edoff, A comparison between thin film solar cells made from co-evaporated $CuIn_{1-x}Ga_xSe_2$ using a one-stage process versus a three-stage process, Prog.Photovoltaics Res. Appl. **23**, 470 (2014).
[5] S. Hwang, L. Larina, H. Lee, S. Kim, K. Choi, C. Jeon, B. Ahn, and B. Shin, Wet pretreatment-induced modification of $Cu(In,Ga)Se_2$/Cd-Free ZnTiO buffer interface, ACS Appl. Mater. Interfaces **10**, 20920 (2018).
[6] S. Kim, H. Yoo, T. Rana, T. Enkhbat, G. Han, J. Kim, S. Song, K. Kim, J. Gwak, Y. Eo, and J. Yun, Effect of crystal orientation and conduction band grading of absorber on efficiency of $Cu(In,Ga)Se_2$ solar cells grown on flexible polyimide foil at low temperature, Adv. Energy Mater. **8**, 1801501 (2018).

[7] S.-H. Wei, S. B. Zhang, and A. Zunger, Effects of Ga addition to $CuInSe_2$ on its electronic, structural, and defect properties, Appl. Phys. Lett. **72**, 3199 (1998).

[8] J. Mattheis, U. Rau, and J. H. Werner, Light absorption and emission in semiconductors with band gap fluctuations - A study on $Cu(In,Ga)Se_2$ thin films, J. Appl. Phys. **101**, 113519 (2007).

[9] J. P. Teixeira, R. A. Sousa, M. G. Sousa, A. F. da Cunha, P. A. Fernandes, P. M. P. Salomé, and J. P. Leitão, Radiative transitions in highly doped and compensated chalcopyrites and kesterites: The case of Cu_2ZnSnS_4, Phys. Rev. B **90**, 235202 (2014).

[10] I. Dirnstorfer, M. Wagner, D. M. Hofmann, M. D. Lampert, F. Karg, and B. K. Meyer, Characterization of $CuIn(Ga)Se_2$ Thin Films, Phys. Status Solidi (A) **168**, 163 (1998).

[11] A. Bauknecht, S. Siebentritt, J. Albert, and M. C. Lux-Steiner, Radiative recombination via intrinsic defects in $Cu_xGa_ySe_2$, J. Appl. Phys. **89**, 4391 (2001).

[12] T. Gokmen, O. Gunawan, T. K. Todorov, and D. B. Mitzi, Band tailing and efficiency limitation in kesterite solar cells, Appl. Phys. Lett. **103**, 103506 (2013).

[13] P. M. P. Salomé, J. P. Teixeira, J. Keller, T. Törndahl, S. Sadewasser, and J. P. Leitão, Influence of CdS and ZnSnO buffer layers on the photoluminescence of $Cu(In,Ga)Se_2$ thin films, IEEE J. Photovoltaics **7**, 670 (2017).

[14] N. Ben Sedrine, R. Ribeiro-Andrade, A. Gustafsson, M. R. Soares, J. Bourgard, J. P. Teixeira, P. M. P. Salomé, M. R. Correia, M. V. B. Moreira, A. G. De Oliveira, J. C. González, and J. P. Leitão, Fluctuating potentials in GaAs:Si nanowires: critical reduction of the influence of polytypism on the electronic structure, Nanoscale **10**, 3697 (2018).

[15] T. Kirchartz, K. Taretto, and U. Rau, Efficiency limits of organic bulk heterojunction solar cells, J. Phys. Chem. C **113**, 17958 (2009).

[16] I. Repins, L. Mansfield, A. Kanevce, S. A. Jensen, D. Kuciauskas, S. Glynn, T. Barnes, W. Metzger, J. Burst, C. Jiang, P. Dippo, S. Harvey, G. Teeter, C. Perkins, B. Egaas, A. Zakutayev, J. Alsmeier, T. Luky, L. Korte, R. G. Wilks, M. Br, Y. Yan, S. Lany, P. Zawadzki, J. Park, and S. Wei, in *2016 IEEE 43rd Photovoltaic Specialists Conference (PVSC)* (IEEE, Portland, OR, USA, 2016), p. 0309.

[17] S. Bourdais, C. Choné, B. Delatouche, A. Jacob, G. Larramona, C. Moisan, A. Lafond, F. Donatini, G. Rey, S. Siebentritt, A. Walsh, and G. Dennler, Is the Cu/Zn disorder the main culprit for the voltage deficit in kesterite solar cells? Adv. Energy Mat. **6**, 1502276 (2016).

[18] J. Jean, T. S. Mahony, D. Bozyigit, M. Sponseller, J. Holovský, M. G. Bawendi, and V. Bulović, Radiative efficiency limit with band tailing exceeds 30% for quantum dot solar cells, ACS Energy Lett. **2**, 2616 (2017).

[19] D. Abou-Ras, N. Schäfer, C. J. Hages, S. Levcenko, J. Márquez, and T. Unold, Inhomogeneities in $Cu(In,Ga)Se_2$ thin films for solar cells: Band-gap versus potential fluctuations, Solar RRL **2**, 1700199 (2018).

[20] T. Kirchartz and U. Rau, What makes a good solar cell? Adv. Energy Mater. **8**, 1703385 (2018).

[21] G. Rey, G. Larramona, S. Bourdais, C. Choné, B. Delatouche, A. Jacob, G. Dennler, and S. Siebentritt, Sol. Energy Mater Sol. Cells **179**, 142 (2018).

[22] H. V. Alberto, R. C. Vilão, R. B. L. Vieira, J. M. Gil, A. Weidinger, M. G. Sousa, J. P. Teixeira, A. F. da Cunha, J. P. Leitão, P. M. P. Salomé, P. A. Fernandes, T. Törndahl, T. Prokscha, A. Suter, and Z. Salman, Slow-muon study of quaternary solar-cell materials: Single layers and *p-n* junctions, Phys. Rev. Mater. **2**, 025402 (2018).

[23] P. M. P. Salomé, R. Ribeiro-Andrade, J. P. Teixeira, J. Keller, T. Törndahl, N. Nicoara, M. Edoff, J. C. González, J. P. Leitão, and S. Sadewasser, Cd and Cu interdiffusion in $Cu(In,Ga)Se_2/CdS$ hetero-interfaces, IEEE J. Photovoltaics **7**, 858 (2017).

[24] H. Guthrey, J. Moseley, J. Nishinaga, H. Shibata, H. Takahashi, and M. Al-Jassim, Spatially resolved recombination analysis of $CuIn_xGa_{1-x}Se_2$ absorbers with alkali post-deposition treatments, IEEE J. Photovoltaics **8**, 1833 (2018).

[25] W. Shockley and H. J. Queisser, Detailed balance limit of efficiency of *p-n* junction solar cells, J. Appl. Phys. **32**, 510 (1961).

[26] J. H. Werner, J. Mattheis, and U. Rau, Efficiency limitations of polycrystalline thin film solar cells: Case of $Cu(In,Ga)Se_2$, Thin Solid Films **480–481**, 399 (2005).

[27] J. K. Larsen, K. Burger, L. Gtay, and S. Siebentritt, in *37th IEEE Photovoltaic Specialists Conference* (IEEE, Portland, OR, USA, 2011), p. 000396.

[28] Reference solar spectral irradiance: Air mass 1.5, astm g173-03, https://www.nrel.gov/grid/solar-resource/spectra-am1.5.html.

[29] U. Rau and J. H. Werner, Radiative efficiency limits of solar cells with lateral band-gap fluctuations, Appl. Phys. Lett. **84**, 3735 (2004).

[30] R. A. J. Janssen and J. Nelson, Factors limiting device efficiency in organic photovoltaics, Adv. Mater. **25**, 1847 (2013).

[31] U. Rau, B. Blank, T. C. M. Müller, and T. Kirchartz, Efficiency Potential of Photovoltaic Materials and Devices Unveiled by Detailed-Balance Analysis, Phys. Rev. Appl. **7**, 044016 (2017).

[32] F. Urbach, The long-wavelength edge of photographic sensitivity and of the electronic absorption of solids, Phys. Rev. **92**, 1324 (1953).

[33] A. L. Efros, Density of states and inter band absorption of light in strongly doped semiconductors, Phys. Usp. **16**, 789 (1974).

[34] J. K. Katahara and H. W. Hillhouse, Quasi-fermi level splitting and sub-bandgap absorptivity from semiconductor photoluminescence, J. Appl. Phys. **116**, 173504 (2014).

[35] G. D. Cody, T. Tiedje, B. Abeles, B. Brooks, and Y. Goldstein, Disorder and the Optical-Absorption Edge of Hydrogenated Amorphous Silicon, Phys. Rev. Lett. **47**, 1480 (1981).

[36] B. I. Shklovskii and A. L. Efros, *Electronic Properties of Doped Semiconductors* (Springer-Verlag, Berlin, 1991).

[37] C. Ulbrich, S. Fahr, J. Üpping, M. Peters, T. Kirchartz, C. Rockstuhl, R. Wehrspohn, A. Gombert, F. Lederer, and U. Rau, Directionalselectivity and ultra-light-trapping in solar cells, Phys. Status Solidi (A) **205**, 2831 (2008).

[38] T. Kirchartz, and U. Rau, in *Advanced Characterization Techniques for Thin Film Solar Cells* (John Wiley & Sons, Ltd, Weinheim, Germany, 2011) Chap. 1, p. 1.

[39] B. Blank, T. Kirchartz, S. Lany, and U. Rau, Selection Metric for Photovoltaic Materials Screening based on Detailed-Balance Analysis, Phys. Rev. Appl. **8**, 024032 (2017).

[40] J. Lindahl, U. Zimmermann, P. Szaniawski, T. Törndahl, A. Hultqvist, P. Salomé, C. Platzer-Björkman, and M. Edoff, Inline $Cu(In,Ga)Se_2$ Co-evaporation for high-efficiency solar cells and modules, IEEE J. Photovoltaics **3**, 1100 (2013).

[41] See Supplemental Material at http://link.aps.org/supplemental/10.1103/PhysRevApplied.11.054013 for the XRD and scanning-electron-microscopy results, a more-detailed explanation of the deconvolution of the PL spectra, the fitting parameters for the EQE plots, and the determination of the value of α_0.

[42] International Centre of Diffraction Data (ICDD). Datasheets: $CuInSe_2$: 04-007-4441; $CuGaSe_2$: 04-005-2518; Mo: 04-001-2734.

[43] J. K. Larsen, S.-Y. Li, J. J. S. Scragg, Y. Ren, C. Hägglund, M. D. Heinemann, S. Kretzschmar, T. Unold, and C. Platzer-Björkman, Interference effects in photoluminescence spectra of Cu_2ZnSnS_4 and $Cu(In,Ga)Se_2$ thin films, J. Appl. Phys. **118**, 035307 (2015).

[44] J. Parravicini, M. Acciarri, M. Murabito, A. L. Donne, A. Gasparotto, and S. Binetti, In-depth photoluminescence spectra of pure CIGS thin films, Appl. Opt. **57**, 1849 (2018).

[45] J. Krustok, J. H. Schön, H. Collan, M. Yakushev, J. Mädasson, and E. Bucher, Origin of the deep center photoluminescence in $CuGaSe_2$ and $CuInS_2$ crystals, J. Appl. Phys. **86**, 364 (1999).

[46] S. B. Zhang, S.-H. Wei, A. Zunger, and H. Katayama-Yoshida, Defect physics of the $CuInSe_2$ chalcopyrite semiconductor, Phys. Rev. B **57**, 9642 (1998).

[47] P. Szaniawski, P. Salomé, V. Fjällström, T. Törndahl, U. Zimmermann, and M. Edoff, Influence of varying Cu content on growth and performance of Ga-graded $Cu(In,Ga)Se_2$ solar cells, IEEE J. Photovoltaics **5**, 1775 (2015).

[48] S. Siebentritt, M. Igalson, C. Persson, and S. Lany, The electronic structure of chalcopyrites-bands, point defects and grain boundaries, Prog. Photovoltaics Res. Appl. **18**, 390 (2010).

[49] P. W. Yu and Y. S. Park, Temperature dependence of photoluminescence from Mg-implanted GaAs, J. Appl. Phys. **48**, 2434 (1977).

[50] J. P. Teixeira, R. A. Sousa, M. G. Sousa, A. F. da Cunha, P. A. Fernandes, P. M. P. Salomé, J. C. González, and J. P. Leitão, Comparison of fluctuating potentials and donor-acceptor pair transitions in a Cu-poor Cu_2ZnSnS_4 based solar cell, Appl. Phys.Lett. **105**, 163901 (2014).

[51] J. P. Teixeira, R. A. Sousa, M. G. Sousa, A. F. da Cunha, P. A. Fernandes, P. M. P. Salomé, J. C. González, and J. P. Leitão, Erratum: "Comparison of fluctuating potentials and donor-acceptor pair transitions in a Cu-poor Cu_2ZnSnS_4 based solar cell" [Appl. Phys. Lett. **105**, 163901 (2014), Appl. Phys. Lett. **107**, 049903 (2015).

[52] M. Lang, C. Zimmermann, C. Krämmer, T. Renz, C. Huber, H. Kalt, and M. Hetterich, Luminescence properties of $Cu_2ZnSn(S,Se)_4$ solar cell absorbers: State filling versus screening of electrostatic potential fluctuations, Phys. Rev. B **95**, 155202 (2017).

[53] P. Van Mieghem, Theory of band tails in heavily doped semiconductors, Rev. Mod. Phys. **64**, 755 (1992).

[54] T. Shioda, S. Chichibu, T. Irie, H. Nakanishi, and T. Kariya, Influence of nonstoichiometry on the Urbach's tails of absorption spectra for $CuInSe_2$ single crystals, J. Appl. Phys. **80**, 1106 (1996).

[55] A. Meeder, D. F. Marrón, A. Rumberg, M. C. Lux-Steiner, V. Chu, and J. P. Conde, Direct measurement of Urbach tail and gap state absorption in $CuGaSe_2$ thin films by photothermal deflection spectroscopy and the constant photocurrent method, J. Appl. Phys. **92**, 3016 (2002).

[56] J. T. Heath, J. D. Cohen, W. N. Shafarman, D. X. Liao, and A. A. Rockett, Effect of Ga content on defect states in $CuIn_{1-x}Ga_xSe_2$ photovoltaic devices, Appl. Phys. Lett. **80**, 4540 (2002).

[57] M. Troviano and K. Taretto, Temperature-dependent quantum efficiency analysis of graded-gap $Cu(In,Ga)Se_2$ solar cells, Sol. Energy Mater Sol. Cells **95**, 3081 (2011).

[58] M. M. Islam, M. A. Halim, T. Sakurai, N. Sakai, T. Kato, H. Sugimoto, H. Tampo, H. Shibata, S. Niki, and K. Akimoto, Determination of deep-level defects in $Cu_2ZnSn(S,Se)_4$ thin-films using photocapacitance method, Appl. Phys. Lett. **106**, 243905 (2015).

[59] C. Malerba M. Valentini, and A. Mittiga, Cation disorder in Cu_2ZnSnS_4 thin films: Effect on solar cell performances, Solar RRL **1**, 1700101 (2017).

[60] S. M. Wasim, C. Rincón, G. Marń, P. Bocaranda, E. Hernández, I. Bonalde, and E. Medina, Effect of structural disorder on the Urbach energy in Cu ternaries, Phys. Rev. B **64**, 195101 (2001).

[61] J. Ramanujam and U. P. Singh, Copper indium gallium selenide based solar cells - a review, Energy Environ. Sci. **10**, 1306 (2017).

[62] J. H. C. Casey and F. Stern, Concentration-dependent absorption and spontaneous emission of heavily doped GaAs, J. Appl. Phys. **47**, 631 (1976).

[63] A. Walsh, J. L. F. Da Silva, and S.-H. Wei, Origins of band-gap renormalization in degenerately doped semiconductors, Phys. Rev. B **78**, 075211 (2008).

[64] B. P. Falcão, J. P. Leitão, M. R. Correia, M. F. Leitão, M. R. Soares, M. V. B. Moreira, A. G. de Oliveira, F. M. Matinaga, and J. C. Gonzaléz, New insights into the temperature-dependent photoluminescence of Mg-doped GaAs nanowires and epilayers, J. Mater. Chem. C **2**, 7104 (2014).

[65] J. Yao, T. Kirchartz, M. S. Vezie, M. A. Faist, W. Gong, Z. He, H. Wu, J. Troughton, T. Watson, D. Bryant, and J. Nelson, Quantifying Losses in Open-Circuit Voltage in Solution-Processable Solar Cells, Phys. Rev. Appl. **4**, 014020 (2015).

[66] R. Scheer, and H. W. Schock, *Chalcogenide Photovoltaics Physics, Technologies, and Thin Film Devices* (Wiley-VCH, Berlim, 2011).

[67] S. De Wolf, J. Holovsky, S.-J. Moon, P. Löper, B. Niesen, M. Ledinsky, F.-J. Haug, J.-H. Yum, and C. Ballif, Organometallic halide perovskites: Sharp optical absorption edge and its relation to photovoltaic performance, J. Phys. Chem. Lett. **5**, 1035 (2014).

[68] P. D. Paulson, R. W. Birkmire, and W. N. Shafarman, Optical characterization of $CuIn_{1-x}Ga_xSe_2$ alloy thin films by spectroscopic ellipsometry, J. Appl. Phys. **94**, 879 (2003).